Applied Materials Today 4 (2016) 1–8

Contents lists available at ScienceDirect

Applied Materials Today

journal homepage: www.elsevier.com/locate/apmt

Cobalt oxide anchored on nitrogen and sulfur dual-doped graphene foam as an effective oxygen electrode catalyst in alkaline media

Xiu-Xiu Ma, Xing-Quan He*

School of Materials Science and Engineering, Changchun University of Science and Technology, Changchun 130022, PR China

ARTICLE INFO

Article history:
Received 14 January 2016
Received in revised form 16 April 2016
Accepted 26 April 2016

Keywords:
Graphene foam
Oxygen reduction reaction
Oxygen evolution reaction
Synergistic effects

ABSTRACT

Developing highly active bifunctional catalysts for oxygen reduction reaction (ORR) and oxygen evolution reaction (OER) in the oxygen electrocatalysis based energy conversion or storage remains challenges. Herein, an efficient catalyst of cobalt oxide (Co_3O_4) nanocrystals grown on nitrogen and sulfur co-doped graphene foam (NSGF) is prepared via a hydrothermal method. Scanning electron microscope (SEM) and transmission electron microscopy (TEM) measurements demonstrate Co_3O_4 is of regular single crystal morphology in the Co_3O_4/NSGF composite with 1:1 mass ratio of cobalt to graphene foam. For ORR, the hybrid favors a direct $4e^-$ pathway, similar to that of Pt/C, but outperforms Pt/C with a long-term durability. Besides, it achieves a small overpotential of ~0.48 V *vs.* SCE at the current density of 10 mA cm^{-2} and there is only 0.018 V *vs.* SCE overpotential increasing after 200 cycles for OER testing. The good electrochemical activities of our fabricated bifunctional catalyst are attributed to electrochemical contributions of the loaded Co_3O_4 nanocrystals, the integral structure of three-dimensional graphene foam, the heteroatoms doping effects and the synergistic effects between Co_3O_4 and NSGF.

1. Introduction

To cater the increasing energy demand and relax the current environment pollution, numerous research has been dedicated to oxygen reaction-based energy conversion and/or storage techniques [1–4]. However, the oxygen reactions suffer from kinetically sluggish problems due to the complex four-electron process, so that catalysts are employed to accelerate oxygen reduction reaction (ORR) and oxygen evolution reaction (OER) processes. Currently, Pt-based alloys and RuO_2 function as the best ORR and OER catalysts, respectively, while their respective OER and ORR performance is poor [5,6]. Besides, these noble metals are scarce, and they face high cost in large-scale applications. Consequently, one of the great challenges being faced is to develop clean, abundant and efficient alternative oxygen electrode catalysts.

To date, the first row transition metals have been studied generally as active electrode materials featured with high catalytic ability for both ORR and OER, such as cobalt and its derives, including mixed-metal oxides [7,8], hydro(oxy) oxides [4,9], phosphates [10], chalcogenides [11,12], and perovskites [3,13]. Among them, Co_3O_4 is popular for affording small overpotential and high stability in alkaline media. Recent theoretical studies have demonstrated that the exposed Co_3O_4 (110), (111) and (311) surface planes are of highly catalytic activity for OER [14–16]. However, the easy aggregation and low conductivity of pure Co_3O_4 decrease the active sites and hamper the transport of electrons during the oxygen reaction process. On the contrary, graphene support with its open ended structure, high electrical conductivity, large surface area and high chemical stability is desirable to derive 3d metal-based composite catalysts [17]. And the combination of Co_3O_4 and heteroatoms doped graphene presented excellent ORR and OER performance [3,13]. For example, several remarkable Co_3O_4-based OER catalysts by adhering them on graphene sheets have been prepared [14,18,19]. When Co_3O_4 anchored on N and/or S-doped graphene, the synergistic effects attributed a lot to the ORR and/or OER abilities [3,13,20–22]. In these cases, nitrogen doping in graphene creates a net positive charge on adjacent carbon atoms to accelerate the adsorption of O_2, and leads to more active sites, larger surface areas, and higher defect density [20,23], facilitating ORR [13,20,22]. Moreover, sulfur doped graphene performed enhanced ORR efficiency due to the nearly electronegativities between sulfur and carbon [10,20,24,25], and the nitrogen and sulfur co-doping generated synergistic effects. However, the structure of cobalt oxide existed differently, and reports on cobalt oxide exposing specific surface planes in catalyzing embedded in nitrogen and sulfur dual-doped 3D graphene as bifunctional catalysts were still not many.

* Corresponding author.
E-mail address: hexingquan@hotmail.com (X.-Q. He).

http://dx.doi.org/10.1016/j.apmt.2016.04.002
2352-9407/

In this study, we successfully prepared a Co_3O_4/NSGF composite, comprising Co_3O_4 single crystals and N, S dual-doped 3D graphene foam (NSGF), via a simple and facile hydrothermal approach using abundant raw resources. Herein, $NH_3{\cdot}H_2O$ acted as both a nitrogen resource and alkali to adjust the pH of the solution (pH > 12) controlling the crystal-particle size and $Na_2S{\cdot}9H_2O$ functioned as a reductive agent and sulfur resource. SEM and TEM methods characterized the formation of Co_3O_4 single crystal on GF in Co_3O_4/NSGF when the mass ratio of Co to GF was 1:1. The hybrid displayed good bifunctional performance as an oxygen electrode catalyst in alkaline media, which was mainly ascribed to heteroatoms doping effects and the synergistic effects between cobalt oxide and graphene foam support.

2. Experimental

2.1. Materials

Graphite powder was purchased from Sinopharm Chemical Reagent Co., Ltd. Pt/C (20 wt%, Pt on Vulcan XC-72) was purchased from Alfa Aesar. 5% Nafion perfluorinated resin solution (in ethanol) and ruthenium (IV) oxide were obtained from Sigma. All of these reagents were analytical grade, and used without further purification, including KOH, $NH_3{\cdot}H_2O$, H_2SO_4, KCl, $NaNO_3$, $KMnO_4$, $Co(OAc)_2{\cdot}4H_2O$, $Na_2S{\cdot}9H_2O$ and $K_3[Fe(CN)_6]$. Ultra pure water was obtained from a Milli-Q water system (18.2 MΩ cm).

2.2. The preparation of GF substrate

In a typical process, graphene oxide (GO) was prepared by oxidation of graphite flakes via a modified Hummers' method [26]. Then, it was dispersed into ultra pure water at a concentration of 30 mg mL^{-1} and subject to freeze-drying process to form the graphene oxide foam, abbreviated as GOF. Next, GOF was first heated to 300 °C with a ramp rate of 1 °C min^{-1}, and then heated up 1050 °C for 5 min at a rate of 10 °C min^{-1} in flowing argon atmosphere. And the cooled product was graphene foam, named as GF.

2.3. The preparation of cobalt oxide/nitrogen, sulfur-doped graphene foam

To fabricate the final catalyst, a hydrothermal method was used. In brief, 23.1 mg of $Co(OAc)_2{\cdot}4H_2O$ was dissolved in ultra pure water and $NH_3{\cdot}H_2O$ was added until the pH of the solution was over 12. The solution was stirred in hot-water conditions for half an hour and cooled to room temperature. Followed by mixing with 2.7 mg of GF in a 1:1 (w/w) ratio (Co atom to GF) and 8.3 mg of $Na_2S{\cdot}9H_2O$, the mixture was sealed to Teflon-lined stainless autoclave at 180 °C for 12 h. The obtained product was subject to freeze-drying, getting the 1:1 Co_3O_4/NSGF cake. By varying the amount of $Co(OAc)_2{\cdot}4H_2O$ to 11.6, 7.7, 46.2 and 69.3 mg, different ratios (Co atom to GF) composites were obtained, corresponding to 1:2 and 2:1 Co_3O_4/NSGF, respectively. For comparative studies, more samples were constructed. The preparations of 1:1 Co_3O_4/SGF (non-nitrogen), Co_3O_4/N (non-graphene foam and sulfur) and NSGF (non-Co_3O_4) were similar to that of 1:1 Co_3O_4/NSGF only by adjusting the amount of the original materials.

2.4. Characterizations of the as-prepared samples

The morphology and structure of as-prepared samples were characterized by scanning electron microscopy (SEM, JSM-6701F, operating at 5 kV) and transmission electron microscopy (TEM, JEOL-2010 transmission electron microscope operating at 200 kV). X-ray powder diffraction (XRD) measurements were taken at ambient temperature with 2θ degree range from 10° to 80° at 40 kV on RIGAK X-ray diffractometer (D/MAX2550 VB/PC, Japan) equipped with Cu Kα radiation (0.15418 Å). Raman spectra were performed on a Tri Vista^{TM}555CRS Raman spectrometer at 785 nm. The Brunauer-Emmett-Teller (BET) surface area and pore volume were evaluated by using nitrogen adsorption-desorption isotherms measured on an ASAP2020 voltric adsorption analyzer at 77 K. X-ray photoelectron spectroscopy (XPS) measurements were carried out on an ESCLAB 250 spectrometer using Al Kα as the exciting source (1486.6 eV photons) to identify the surface chemical composition and bonding state.

2.5. Preparation of modified electrodes

Prior to modification, the working electrode was polished successively with 1.0, 0.3 and 0.05 mm aluminum oxide slurry, then ultrasonically rinsed with distilled water, absolute ethanol and distilled water in turn. Afterwards, the cleaned glassy carbon (GC) electrode was blow-dried with N_2 at ambient temperature. In order to modify the GC electrode, a homogeneous ink was prepared by mixing 4.0 mg of catalyst, 1.5 μL of 5 wt% Nafion solution and 2.0 mL of ethanol with the aid of ultrasonic vibration. A certain amount of catalyst ink was pipetted onto the GC electrode, and then dried in the air to hold the attachment of the film to the electrode surface. The catalyst loading per area on the GC electrode was always kept to be 0.212 mg cm^{-2}. For comparison, the same amount of 1:1 Co_3O_4/N, NSGF, 1:1 Co_3O_4/SGF or Pt/C was also loaded onto the GC electrode.

2.6. Electrochemical measurements of the samples

Cyclic voltammetry (CV) measurements were performed with a CHI 660E electrochemical workstation (CH Instruments, Shanghai CHENHUA company) in a conventional three-electrode cell using the coated GC electrode (3 mm in diameter) as the working electrode, a platinum wire as the auxiliary electrode, and a saturated calomel electrode (SCE) as the reference electrode. Rotating disk electrode (RDE, 5 mm in diameter), rotating ring disk electrode (RRDE, 5.61 mm in diameter) and current-time (*i*-*t*) chronoamperometry measurements were carried out with a Pine Instrument Company AF-MSRCE modulator speed rotator on a CHI 660E electrochemical workstation with a standard three-electrode system. CV measurements for the ORR were operated at the scan rate of 10 mV s^{-1} in an O_2/N_2-saturated 0.1 M KOH solution. RDE and RRDE measurements for the ORR were performed at the scan rate of 10 mV s^{-1} in an O_2-saturated 0.1 M KOH solution, and the RDE electrode was polished by 0.3 and 0.05 mm aluminum oxide slurry and RRDE was only dealt with 0.05 mm aluminum oxide slurry. For RRDE measurements, the collection efficiency of platinum ring was 37.0%. CV and RDE measurements for the OER were carried out at the scan rate of 10 mV s^{-1} in a N_2-saturated 0.1 M KOH solution. All electrochemical measurements were performed 3 times to avoid any incidental error and all potentials in this study were reported relative to the saturated calomel electrode (SCE).

3. Results and discussion

3.1. Characterizations of Co_3O_4/NSGF composites

Fig. 1a depicts XRD patterns of the synthesized samples. Pure GF sample exhibited a broad diffraction peak (005) at $2\theta = 25.8°$. In the case of 1:1 Co_3O_4/NSGF hybrid, the (111), (220), (311), (222), (400), (422), (440) and (511) peaks matched well with those of cubic Co_3O_4 (PDF-#78-1969). And Co_3O_4 were also formed in 1:2 and 2:1 Co_3O_4/NSGF composites. The strong peaks suggested the high crystallinity of Co_3O_4 nanoparticles (NPs). The nitrogen adsorption-desorption isotherm (Fig. 1b) assessing the porous nature clearly

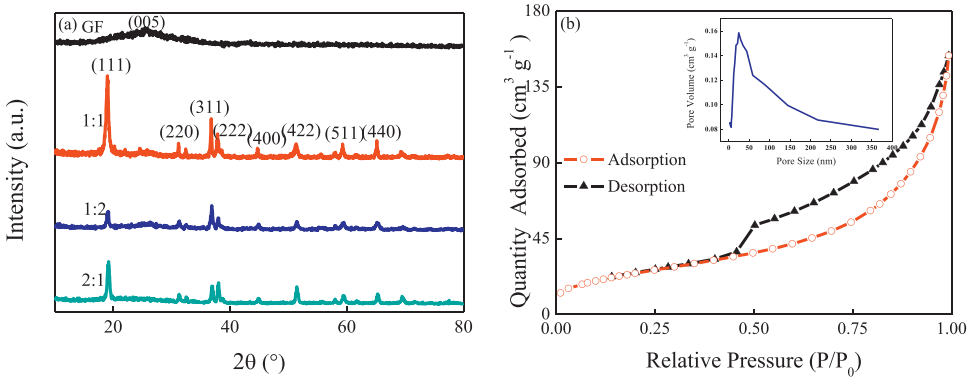

Fig. 1. (a) XRD patterns of GF, 1:1, 1:2 and 2:1 Co_3O_4/NSGF and (b) nitrogen adsorption-desorption isotherms of 1:1 Co_3O_4/NSGF (inset: corresponding pore size distribution from the adsorption branch).

shows a type isotherm IV indicative of the existence of mesopores and macropores. The average pore size in the pore size distribution curve (Fig. 1b inset) was around 82.3 nm and tC-S-Che BET surface area was 90.2 $m^2\ g^{-1}$, resulting from the occurrence of partial pore blockage [27].

Details of the morphology and structure of the hybrids were characterized by SEM and TEM. Both graphene foam (GF) and graphene oxide foam (GOF) exhibit intense interconnected network morphology (Fig. 2a and b). For 1:1 Co_3O_4/NSGF, cubic Co_3O_4 NPs were observed on the GF sheets or in the holes (Fig. 2c, d and f). While the Co_3O_4 particles did not grow well in 1:2 and 2:1 Co_3O_4/NSGF composites (see Supporting information Fig. S1a and b). TEM images showed that the GOF and the GF were crumbled with covered sheets (Supplementary Fig. S1c, Fig. 2e, agreeing well with SEM results. The high-resolution TEM (HRTEM) image given in Fig. 2g clearly displays that lattice fringe spacing of Co_3O_4 was around 0.27 nm, and the selected area electron diffraction (SAED) pattern (the inset in Fig. 2h) demonstrated Co_3O_4 was of single crystalline form, and the first diffraction areas corresponded to (111) surface plane of Co_3O_4. Details of study have demonstrated that the exposed Co_3O_4 (111) surface contributed a lot to OER [3,13].

Raman spectra of GO, GOF and Co_3O_4/NSGF composites all presented the D bands located around 1340 cm^{-1} (arise from sp^3 defect sites) and the G bands around 1589 cm^{-1} (attribute to sp^2-bonded pairs) (Fig. 3a). The I_D/I_G values used to gauge structure disorder of the GOF, GF and Co_3O_4/NSGF samples increased notably when compared with that of GO (Fig. 3b, Supplementary Fig. S2a), indicating the altered structure of GO [13]. Besides, the D bands had a slight blue shift and the G bands had a mild red shift, suggesting the occurrence of electron transfer from graphene to the anchored electron-accepting Co_3O_4 [3,15]. XPS survey spectrum for the 1:1 Co_3O_4/NSGF composite contained the expected C, O, Co, N and S elements (Fig. 3c), confirming the successful cobalt, nitrogen and sulfur introducing. It is generally believed that N destroys the electric neutrality of carbon plane structure, creates positive charges on the neighbor carbon atoms, and improves the graphene to donate electrons to O_2, which is the acceleration of graphene materials to be excellent ORR catalyst [15]. In addition, nitrogen promoted sulfur and cobalt doping (Table 1) [20,22]. The addition of sulfur as a co-dopant is highly beneficial for ORR [20]. The C 1s lever peaks of 1:1 Co_3O_4/NSGF were resolved into three components centered at 284.5, 285.0 and 286.5 eV, assigned to sp^2C-sp^2C, N-$sp^{2(3)}$C and S—C bonds (Fig. 3d) [20,28]. Similarly, the S 2p signals were deconvoluted into four components centered at 162.0, 164.0, 167.9 and 169.1 eV, representing C—S—C, thiophenic S, –SO— and inorganic S (Supplementary Fig. S2b). The peak at 164.0 eV strongly revealed the presence of nitrogen and sulfur incorporated on the composite [29]. N 1 s peaks were fitted to 398.3, 399.9 and 401.8 eV, attributing to pyridinic, pyrrolic and graphitic N atoms (Fig. 3e) [15,20,22]. Co $2p_{3/2}$ and Co $2p_{1/2}$ were located at 780.5 eV and 796.0 eV (Fig. 3f). Thiophenic S, pyridinic and graphitic N atoms were catalytic active sites [10,20,22,30–32], which reduced the band gap of the graphene and contributed a lot to ORR activity. To assess the nitrogen-doped influence, the 1:1 Co_3O_4/SGF was characterized. Compared the 1:1 Co_3O_4/SGF XPS spectrum, the binding energy of C 1s spectral line in 1:1 Co_3O_4/NSGF had a slight negative shift (0.1 eV), while that of Co 2p positively shifted a lot (0.6 eV), identifying the influence of nitrogen atom on the binding energy of Co 2p (Table 1).

3.2. Catalysis of Co_3O_4/NSGF composites for ORR

To evaluate the ORR catalytic activity, CV testings were first carried out for 1:1 Co_3O_4/NSGF in N_2-saturated 0.1 M KOH electrolyte in the potential window from 0.2 V to −0.7 V *vs.* SCE, and only a featureless voltammogram was obtained. Whereas in the presence of O_2, a well defined ORR peak was observed, suggesting the electrocatalytic activity of 1:1 Co_3O_4/NSGF towards ORR (Fig. 4a). When different ratios of materials were tested for CV performance at the same catalyst loading of 0.212 mg cm^{-2} (Fig. 4b), 1:1 composite exhibited the largest current density and relatively positive reduction potential, therefore, it is the object during the entire study. In Fig. 4c, all of NSGF, Co_3O_4/N and 1:1 Co_3O_4/SGF showed small current densities, while the current density of increased in 1:1 Co_3O_4/NSGF, demonstrating the synergistic effects between Co_3O_4 and NSGF [21,22].

For better understanding the mechanism of the catalytic system, the catalytic activity was studied using rotating disk electrode, as well as the rotating ring disk electrode. LSV curves of the 1:1 sample were collected on the RDE at a scan rate of 10 mV s^{-1} in O_2-saturated 0.1 M KOH electrolyte. Typically, increasing reaction currents were observed with increasing the rotation speeds at ranges from 800 rpm to 2500 rpm (Fig. 4d) due to the shortened oxygen diffusion distance under high rotating rate. Fig. 4e shows the corresponding Koutecky-Levich plots with the inverse current density (J^{-1}) versus the inverse of the square root. The linearity of the Koutecky-Levich plots and the near parallelism of the fitting lines suggested first-order reaction kinetics toward the concentration of dissolved oxygen and the similar electron transfer number in ORR at different potentials [33,34]. The average electron transferred number (n) per oxygen was about 3.7 (Supplementary Fig. S3a) according to the corresponding Koutecky-Levich plots (J^{-1} *vs.* $\omega^{-1/2}$) at various electrode potentials which was calculated based on Koutecky-Levich equations [33], similar to that (3.9) of Pt/C, indicating a direct 4e$^-$ oxygen reduction process. Besides, it performed similar ORR properties compared with Pt/C at the same catalyst loading just for LSV curves at 1600 rpm (Supplemen-

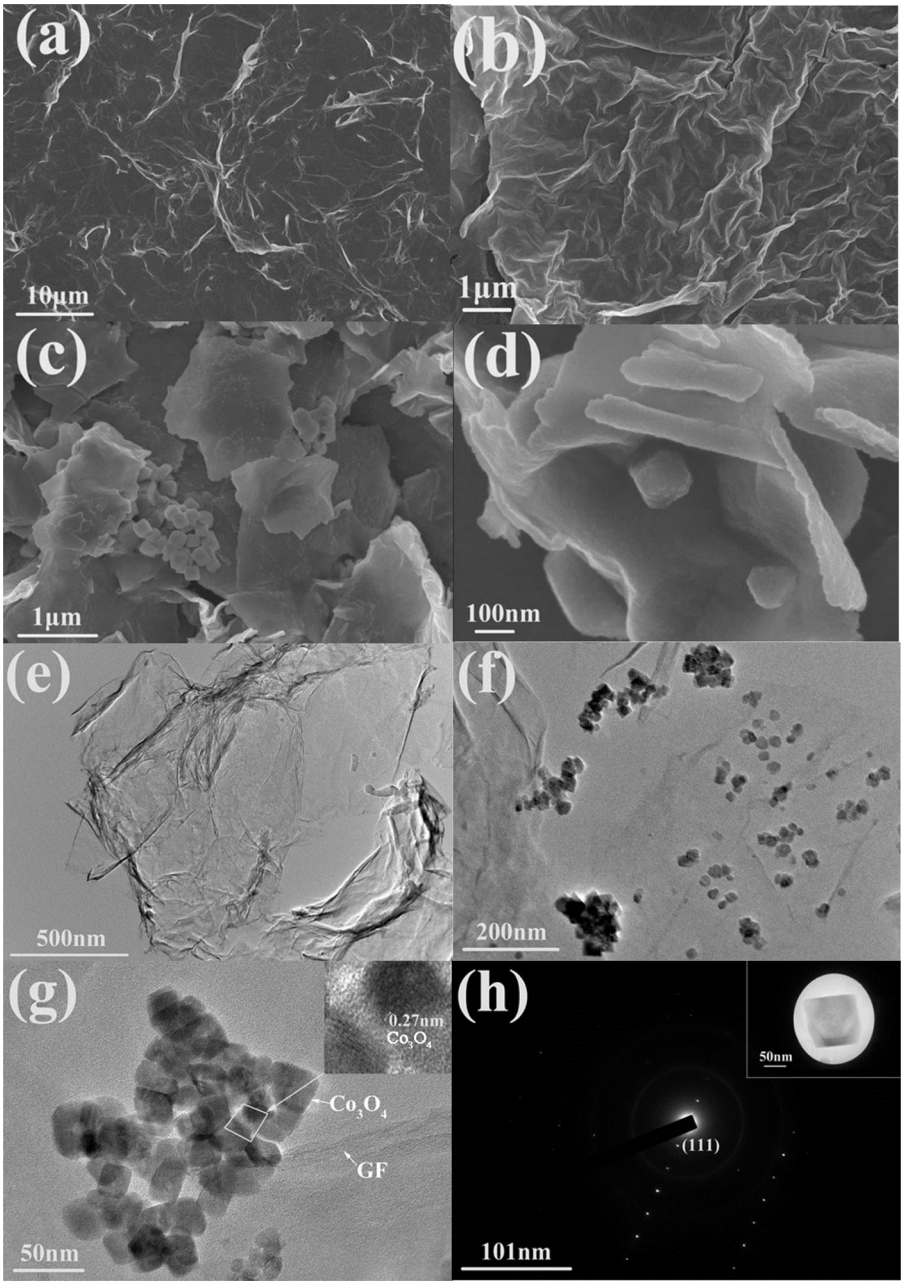

Fig. 2. (a–d) SEM images of (a) graphene oxide foam (GOF), (b) graphene foam (GF), (c,d) 1:1 Co_3O_4/NSGF and (e–h) TEM images of (e) graphene foam (GF), (f) 1:1 Co_3O_4/NSGF, (g) HRTEM of 1:1Co_3O_4/NSGF with the inset exhibiting the lattice fringe spacing of the selected area and (h) SAED of 1:1 Co_3O_4/NSGF with the inset showing the single Co_3O_4 NPs.

Table 1
Elemental analysis of the XPS spectra.

	1:1 Co_3O_4/NSGF		1:1 Co_3O_4/SGF	
	Binding Energy (eV)	At.%	Binding Energy (eV)	At.%
C 1s	284.6	74.1	284.7	88.8
O 1s	531.0	18.2	532.2	9.6
S 2P	168.5	3.0	164.0	0.4
Co 2p	780.5	4.1	779.9	1.2
N 1s	399.7	0.6	–	–

tary Fig. S3b). Tafel polarization plots were analyzed from the LSV curves at 1600 rpm of 1:1 composite. Table 2 shows the slopes were 186.4 mV dec^{-1} and 51.8 mV dec^{-1} at the high and low overpotential regions, corresponding to diffusion control and kinetic control, respectively. And the slope of 51.8 mV dec^{-1} was close to that (47.0 mV dec^{-1}) of Pt/C, demonstrating the intrinsic quick kinectic activity. To verify the ORR catalytic pathways, RRDE measurements were carried out to monitor the formation of HO_2^-% during the ORR process (Fig. 4f). It can be clearly seen that 1:1 Co_3O_4/NSGF exhibited an onset potential of −0.05 V *vs.* SCE, closed to that (-

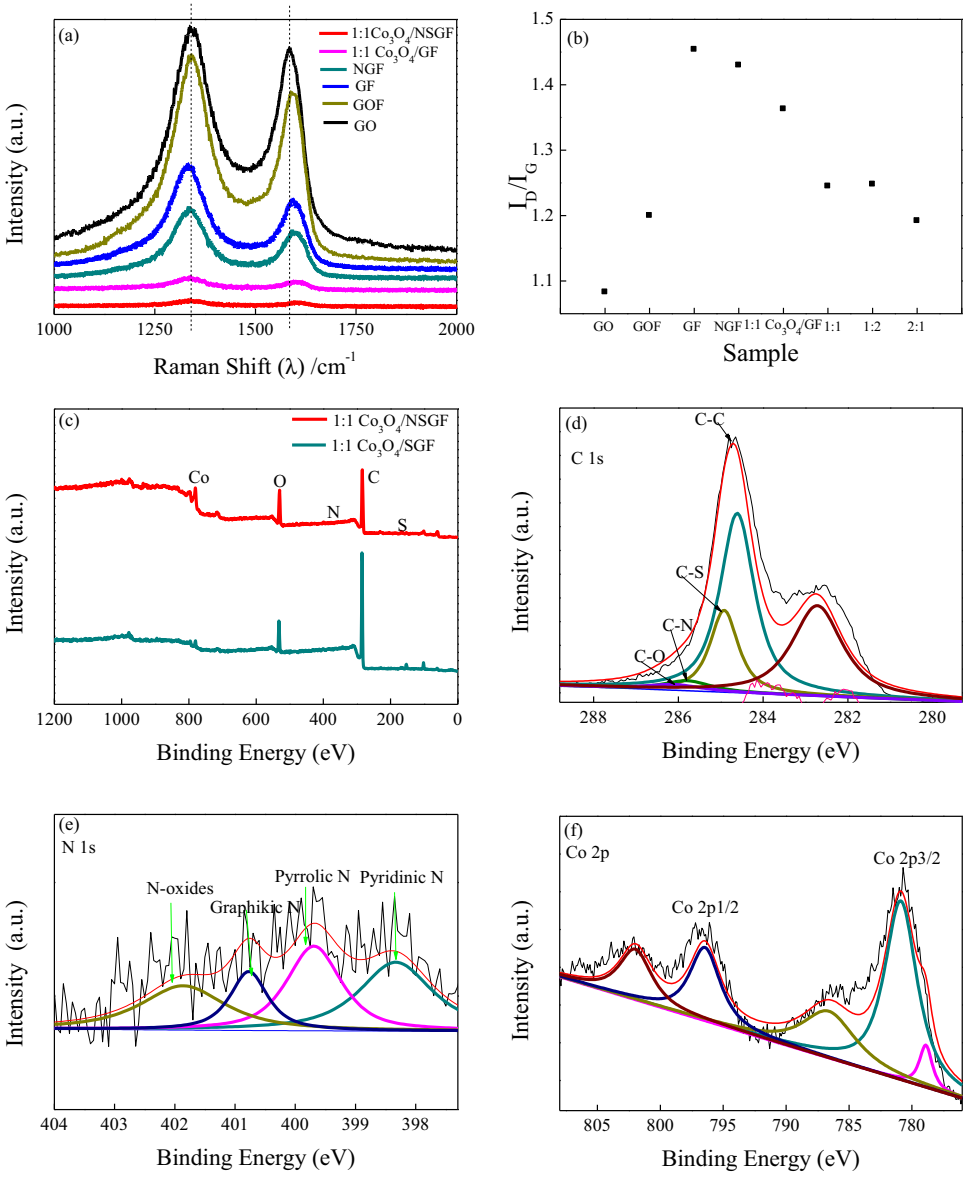

Fig. 3. (a) Raman spectra of the various catalysts and (b) the I_D/I_G distributions of various catalysts; XPS spectra of the (c) 1:1 Co_3O_4/NSGF and 1:1 Co_3O_4/SGF and (d–f) the high resolution spectra of C 1s, N1s and Co 2p for 1:1Co_3O_4/NSGF.

Table 2
Comparison of Tafel slopes for different catalysts towards ORR.

	Tafel Slope/(mV dec^{-1})	
	High Overpotential Region	Low Overpotential Region
1:1 Co_3O_4/NSGF	186.4	51.8
20 wt% Pt/C	145.4	47.0

0.02 V *vs.* SCE) of Pt/C, but outperformed Pt/C with a more positive half-wave potential ($\Delta E_{1/2}$~ 0.034 V *vs.* SCE). By studying the ring and disk current densities, the HO_2^- yield for 1:1 Co_3O_4/NSGF was below 15.0% at a potential range of −0.3 to −0.7 V *vs.* SCE and corresponded to a high electron transferred number of around 3.7, as shown in Fig. S3c, in which the HO_2^- yield and the electron transfer number (n) can be calculated according to Eqs. (1) and (2) [33],

$$HO_2^-\% = 200 \times \frac{i_R/N}{i_D + i_R/N} \quad (1)$$

$$n = \frac{4i_D}{i_D + i_R/N} \quad (2)$$

where, i_D is the disk current, i_R is the ring current, and N is the current collection efficiency of the Pt ring.

RRDE tests agreed well with our results calculated from the Koutecky-Levich equations that the ORR electron transferred number per oxygen for 1:1 Co_3O_4/NSGF was close to 4, further suggesting the ORR process on 1:1 Co_3O_4/NSGF catalyst proceeded via a $4e^-$ pathway. In contrast, the 1:1 Co_3O_4/SGF, Co_3O_4/N and NSGF electrodes displayed more HO_2^-% production and much lower n values of 3.4, 3.1 and 3.1, respectively, indicating the 2 + 2 electron transfer pathways dominated the ORR process (see Fig. S3d–f) [22,35].

In addition to the catalyst activity, catalyst stability is another critical issue that needs to take into consideration. The corresponding current-time (i-t) chronoamperometric measurements of 1:1 Co_3O_4/NSGF at −0.34 V *vs.* SCE remained current retention as high as 87.0% over 10000 s in an O_2-saturated 0.1 M KOH solution under 1600 rpm, outperforming that (74.0%) of Pt/C, as shown in Supple-

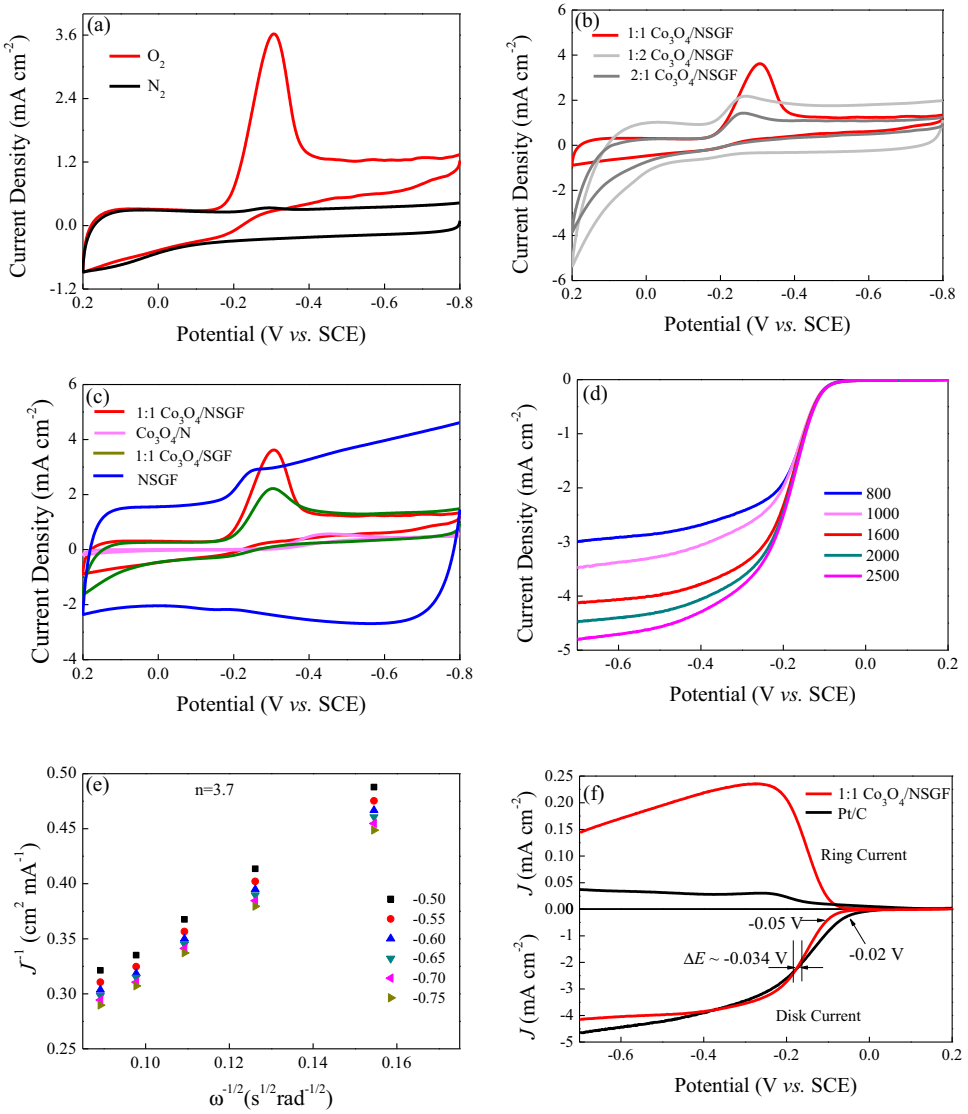

Fig. 4. CV results of (a) the 1:1 Co_3O_4/NSGF at O_2/N_2-saturated 0.1 M KOH as the electrolyte with a scan rate of 10 mV s^{-1}, (b) Co_3O_4/NSGF at different mass ratios, (c) various comparable samples; (d) the RDE testing results of the 1:1 Co_3O_4/NSGF for various rotation speeds, (e) K-L plot fitting results, and (f) RRDE measurements recorded at 10 mV s^{-1} with a rotating speed of 1600 rpm in O_2-saturated 0.1 M KOH with the ring electrode polarized at 0.2 V *vs.* SCE.

mentary Fig. S3g. Other than the outstanding long-term durability, the 1:1 Co_3O_4/NSGF hybrid also showed less sensitive to methanol crossover effects than that of Pt/C, see Fig. S3h. According to the above, the 1:1 Co_3O_4/NSGF hybrid favored a $4e^-$ pathway in catalyzing ORR and exhibited intrinsic long-term durability, it opens a way to be a promising candidate to the ORR catalyst.

3.3. *Electrochemical impedance spectroscopy (EIS) studies on the samples*

Electrochemical impedance spectroscopy (EIS) is one of the powerfully electrochemical techniques to be used to analyse electrode kinetics [36,37]. Herein, EIS patterns were taken in the frequency range of 1 MHz–0.01 Hz. Nyquist (Z' *vs.* −Z") plots of the samples including GF, 1:1 Co_3O_4/NSGF, 1:1 Co_3O_4/SGF and 1:1 Co_3O_4/NGF were shown in Fig. 5. The silent features of impedance studies were the semicircle curves, and the semicircle radius became larger following the increasing order of GF, 1:1 Co_3O_4/NSGF, 1:1 Co_3O_4/SGF and 1:1 Co_3O_4/NGF as presented in Fig. 5, suggesting the lowered resistance. The semicircle at low frequency was due to the bulk resistance, at medium frequency

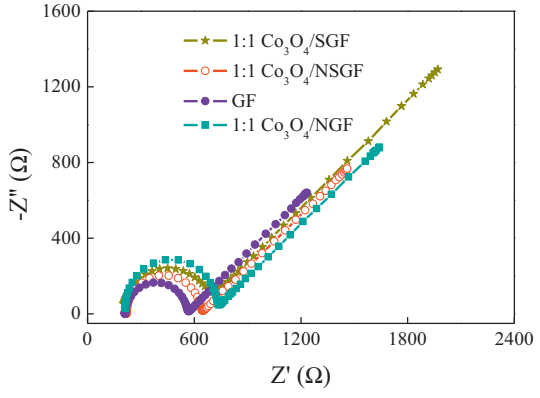

Fig. 5. Electrochemical imedance spectroscopies for GF, 1:1 Co_3O_4/NSGF, 1:1 Co_3O_4/SGF and 1:1 Co_3O_4/NGF at the frequency range from 1 MHz to 0.01 Hz.

implied the charge transfer resistance assigned to the electrolyte-electrode interface, and at high frequency is surface film impedance [36–38]. The fitted impedance values were obtained using equiva-

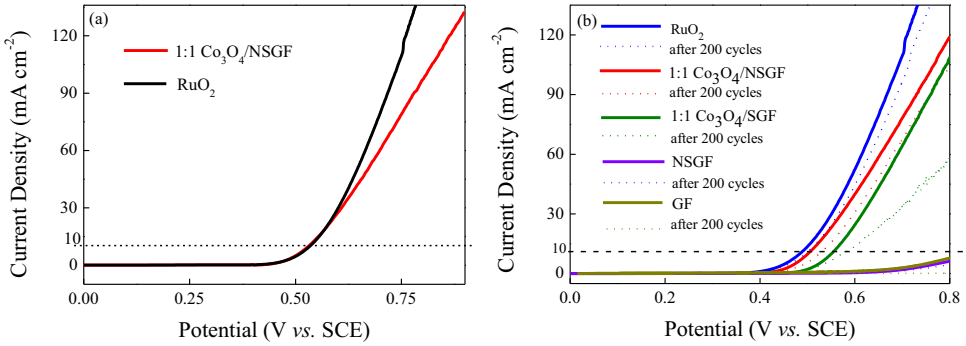

Fig. 6. OER testing results recorded (a) LSV results of 1:1 Co_3O_4/NSGF and RuO_2, (b) LSV curves of 1:1 Co_3O_4/NSGF, 1:1 Co_3O_4/SGF, NSGF, GF and RuO_2 before and after 200 cycles at rotating speed of 1600 rpm in N_2-saturated 0.1 M KOH.

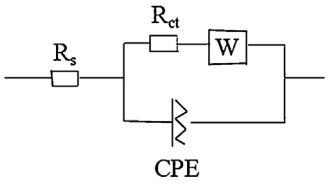

Scheme 1. Equivalent electrical circuit for Nyquist plots.

Table 3
Fitted impedance values of the investigated samples.

	R_s (Ω)	R_{ct} (Ω)
GF	219	419
1:1 Co_3O_4/NSGF	219	443
1:1 Co_3O_4/SGF	214	476
1:1 Co_3O_4/NGF	215	515

Table 4
Comparison of OER parameters for different catalysts.

Catalysts	Onset Potential (V *vs.* SCE)	η@J = 10 mA cm^{-2} (V *vs.* SCE)	Tafel Slope (mV dec^{-1})
1:1 Co_3O_4/NSGF	0.46	0.48	52.9
RuO_2	0.44	0.37	69.0

lent electrical circuit model (see Scheme 1), which were comprised of a R_s (electrolyte resistance), R_{ct} (charge transfer resistance), W (Warburg impedance) and CPE (double layer capacitance), and the impedance values were given in Table 3. Generally, the impedance value was sensitive to the nature and crystal structure of the materials. It can be seen in Table 3 that the 1:1 Co_3O_4/NSGF hybrid performed a larger impedance value than that of GF, but deserved a lower value than those of 1:1 Co_3O_4/SGF and 1:1 Co_3O_4/NGF, demonstrating the quick electrode kinetics of the 1:1 Co_3O_4/NSGF composite and the synergistic effects in the mean time.

3.4. *Catalysis of Co_3O_4/NSGF composites for OER*

To be used as bi-functional catalysts for transition-metal-based hybrids, OER activities were estimated by LSV curves. LSV characterization in Fig. 6a demonstrated that the current density of 1:1 Co_3O_4/NSGF at 0.75 V *vs.* SCE was much smaller than that of RuO_2, but the OER onset potential of 1:1 Co_3O_4/NSGF was 0.46 V *vs.* SCE, very close to that (0.44 V *vs.* SCE) of RuO_2 (Table 4). It is very meaningful to compare the overpotential η requirement for achieving the current density of 10 mA cm^{-2}, which was a metric relevant to solar fuel synthesis [39]. Notably, the catalyst composite could afford such current density at a small η of ~480 mV *vs.* SCE, close to that for RuO_2 (Table 4). The OER kinetics of the samples were probed by corresponding Tafel plots (log j–η), as shown in Table 4. The Tafel slope value for 1:1 Co_3O_4/NSGF was 52.9 mV dec^{-1}, smaller than 69.0 mV dec^{-1} for RuO_2, close to other state of Co-based OER catalysts, such as 75 mV dec^{-1} for CoS_2(400)/N,S-GO [40], 62 mV dec^{-1} for $Co(OH)_2$ [41], and 72 mV dec^{-1} for Co_3O_4/N-porous carbon [3], indicating the compound is of outstanding intrinsic OER kinetics.

Other than high OER activity, long-term stability is another critical indicator in the practical application of electrode materials, so we further performed continuous potential cycles of the 1:1 Co_3O_4/NSGF, 1:1 Co_3O_4/SGF, NSGF, GF and RuO_2 in N_2-saturated 0.1 M KOH. Fig. 6b shows that after 200 cycles, there was only 18 mV potential increase for the resultant 1:1 Co_3O_4/NSGF at the current density of 10 mA cm^{-2}, which did comparative durability to RuO_2, but outperformed the others. The excellent performance of 1:1 Co_3O_4/NSGF for ORR and OER was attributed to the strong synergistic effects between Co_3O_4 and NSGF and the single crystalline structure of Co_3O_4 exposing the special (111) plane, as NGF did not affect the OER activity [42].

All in all, the 1:1 Co_3O_4/NSGF hybrid exhibited a quick four electron transfer pathway toward ORR, but outperformed Pt/C with long-term durability and insensitive to methanol. Additionally, it displayed good OER activities which were comparable with RuO_2, even closed to the state-of-the-art nonprecious catalysts. The doping effects of the heteroatoms (nitrogen and sulfur), the integrated structure of graphene foam, the exposed Co_3O_4 (111) plane and the synergistic effects between cobalt oxide and N,S dual-doped graphene foam contributed a lot to the oxygen reduction reaction and oxygen evolution reaction.

4. Conclusions

In summary, we have successfully constructed the Co_3O_4 nanocrystals supported on N, S-codoped graphene foam via a green hydrothermal method using inexpensive precursors. 1:1 Co_3O_4/NSGF exhibits good bifunctional performance for oxygen electrodes. The improved electrochemical performance and cycle stability of the 1:1 Co_3O_4/NSGF hierarchical hybrids are attributed to the intimate integration of GF, N and S doping effects, the exposure of Co_3O_4 (111) plane and the strong synergistic effects between the Co_3O_4 and GF. We believe that the as-prepared 1:1 Co_3O_4/NSGF is a promising candidate to the oxygen electrode catalyst in alkaline media.

Acknowledgments

The authors acknowledge the support from the Nature Science Foundation of China (NFSC-NO. 21273024), and Nature Science Foundation of Jinlin Province, China (NO.20160101298 JC).

Appendix A. Supplementary data

Supplementary data associated with this article can be found, in the online version, at http://dx.doi.org/10.1016/j.apmt.2016.04.002.

References

[1] M. Guarnieri, P. Alotto, F. Moro, Modeling the performance of hydrogen–oxygen unitized regenerative proton exchange membrane fuel cells for energy storage, J. Power Sources 297 (2015) 23–32.
[2] I. Katsounaros, S. Cherevko, A.R. Zeradjanin, K.J.J. Mayrhofer, Oxygen electrochemistry as a cornerstone for sustainable energy conversion, Angew. Chem. Int. Ed. 53 (2014) 102–121.
[3] Y. Hou, J.Y. Li, Z.H. Wen, S.M. Cui, C. Yuan, J.H. Chen, Co_3O_4 nanoparticles embedded in nitrogen–doped porous carbon dodecahedrons with enhanced electrochemical properties for lithium storage and water splitting, Nano Energy 12 (2015) 1–8.
[4] Y. Zhan, G.J. Du, S.L. Yang, C.H. Xu, M.H. Lu, Z.L. Liu, J.Y. Lee, Development of cobalt hydroxide as a bifunctional catalyst for oxygen electrocatalysis in alkaline solution, ACS Appl. Mater. Interfaces 7 (2015) 12930–12936.
[5] V.T.T. Ho, N.G. Nguyen, C.J. Pan, J.H. Cheng, J. Rick, W.N. Su, J.F. Lee, H.S. Sheu, B.J. Hwang, Advanced nanoelectrocatalyst for methanol oxidation and oxygen reduction reaction, fabricated as one-dimensional Pt nanowires on nanostructured robust $Ti_{0.7}Ru_{0.3}O_2$ support, Nano Energy 1 (2012) 687–695.
[6] S. Trasatti, Electrocatalysis in the anodic evolution of oxygen and chlorine, Electrochim. Acta 29 (1984) 1503–1512.
[7] L. Chen, J.H. Yang, S.N. Klaus, L.J. Lee, R. W.-Robinson, J. Ma, Y.W. Lum, J.K. Cooper, F.M. Toma, L.W. Wang, I.D. Sharp, A.T. Bell, J.W. Ager, P–type transparent conducting oxide/n–type semiconductor heterojunctions for efficient and stable solar water oxidation, J. Am. Chem. Soc. 137 (2015) 9595–9603.
[8] X.J. Cui, P.J. Ren, D.H. Deng, J. Deng, X.H. Bao, Single layer graphene encapsulating non-precious metals as high–performance electrocatalysts for water oxidation, Energy Environ. Sci. (2015).
[9] Z.L. Zhao, H.X. Wu, H.L. He, X.L. Xu, Y.D. Jin, A high–performance binary Ni–Co hydroxide–based water oxidation electrode with three–dimensional coaxial nanotube array structure, Adv. Funct. Mater. 24 (2014) 4698–4705.
[10] J.J. Duan, S. Chen, M. Jaroniec, S.Z. Qiao, Heteroatom–doped graphene-based materials for energy–relevant electrocatalytic processes, ACS Catal. 5 (2015) 5207–5234.
[11] B.L. Chen, R. Li, G.P. Ma, X.L. Gou, Y.Q. Zhu, Y.D. Xia, Cobalt sulfide/N,S codoped porous carbon core–shell nanocomposites as superior bifunctional electrocatalysts for oxygen reduction and evolution reactions, Nanoscale 7 (2015) 20674–20684.
[12] P.D. Ganesan, M. Prabu, J. Sanetuntikul, S. Shanmugam, Cobalt sulfide nanoparticles grown on nitrogen and sulfur codoped graphene oxide: an efficient electrocatalyst for oxygen reduction and evolution reactions, ACS Catal. 5 (2015) 3625–3637.
[13] S.K. Singh, V.M. Dhavale, S. Kurungot, Low surface energy plane exposed Co_3O_4 nanocubes supported on nitrogen–doped graphene as an electrocatalyst for efficient water oxidation, ACS Appl. Mater. Interfaces 7 (2015) 442–451.
[14] J.Z. Zhu, X.D. Ren, J.J. Liu, W.Q. Zhang, Z.Y. Wen, Unraveling the catalytic mechanism of Co_3O_4 for the oxygen evolution reaction in a Li–O_2 Battery, ACS Catal. 5 (2015) 73–81.
[15] X.M. Ge, A. Sumboja, D. Wuu, T. An, B. Li, F.W.T. Goh, T.S.A. Hor, Y. Zong, Z.L. Liu, Oxygen reduction in alkaline media: from mechanisms to recent advances of catalysts, ACS Catal. 5 (2015) 4643–4667.
[16] Y.X. Zhang, F. Ding, C. Deng, S.Y. Zhen, X.Y. Li, Y.F. Xue, Y.M. Yan, K.N. Sun, Crystal plane–dependent electrocatalytic activity of Co_3O_4 toward oxygen evolution reaction, Catal. Commun. 67 (2015) 78–82.
[17] T.Y. Ma, S. Dai, M. Jaroniec, S.Z. Qiao, Metal–organic framework derived hybrid Co_3O_4-carbon porous nanowire arrays as reversible oxygen evolution electrodes, J. Am. Chem. Soc. 136 (2014) 13925–13931.
[18] Y.Y. Fang, X.Z. Li, Y.P. Hu, F. Li, X.Q. Lin, M. Tian, X.C. An, Y. Fu, J. Jin, J.T. Ma, Ultrasonication-assisted ultrafast preparation of multiwalled carbon nanotubes/Au/Co_3O_4 tubular hybrids as superior anode materials for oxygen evolution reaction, J. Power Sources 300 (2015) 285–293.
[19] L.J. Li, S.Y. Liu, A. Manthiram, Co_3O_4 nanocrystals coupled with O- and N-doped carbon nanoweb as a synergistic catalyst for hybrid Li-air batteries, Nano Energy 12 (2015) 852–860.
[20] L.M. Dai, Y.H. Xue, L.T. Qu, H.J. Choi, J.B. Baek, Metal–free catalysts for oxygen reduction reaction, Chem. Rev. 115 (2015) 4823–4892.
[21] Y.Y. Liang, Y.G. Li, H.L. Wang, J.G. Zhou, J. Wang, T. Regier, H.J. Dai, Co_3O_4 nanocrystals grown on graphene: a new bifuncationl catalyst for oxygen reduction and evolution, Nat. Mater. 10 (2011) 780–786.
[22] N. Yao, L. Li, Z.D. Wei, Recent advancements in Pt and Pt-free catalysts for oxygen reduction reaction, Chem. Soc. Rev. 44 (2015) 2168–2201.
[23] S.S. Yu, Q.B. Wen, W.T. Zheng, Q. Jiang, First principle calculations of the electronic properties of nitrogen-dopedcarbon nanoribbons with zigzag edges, Carbon 46 (2008) 537–543.
[24] Z. Yang, Z. Yao, G.F. Li, G.Y. Fang, H.G. Nie, Z. Liu, X.M. Zhou, X. Chen, S.M. Huang, Sulfur–doped graphene as an efficient metal–free cathode catalyst for oxygen reduction, ACS Nano 6 (2012) 205–211.
[25] I.Y. Jeon, H.J. Choi, S.M. Jung, J.M. Seo, M.J. Kim, L.M. Dai, J.B. Baek, Large–scale production of edge–selectively functionalized graphene nanoplates via ball milling and their use as metal–free electrocatalysts for oxygen reduction reaction, J. Am. Chem. Soc. 135 (2013) 1386–1393.
[26] X.T. Zhang, Z.Y. Sui, B. Xu, S.F. Yue, Y.J. Luo, W.C. Zhan, B. Liu, Mechanically strong and highly conductive graphene aerogel and its use as electrodes for electrochemical power sources, J. Mater. Chem. 21 (2011) 6494–6497.
[27] Y.F. Yang, L.T. Jia, B. Hou, D.B. Li, J.G. Wang, Y.H. Sun, The correlation of interfacial interaction and catalytic performance of N–doped mesoporous carbon supported cobalt nanoparticles for Fischer–Tropsch synthesis, J. Phys. Chem. C 118 (2014) 268–277.
[28] L. Liu, S.M. Ryu, M.R. Tomasik, E. Stolyarova, N. Jung, M.S. Hybersten, M.L. Steigerwald, L.E. Brus, G.W. Flynn, Graphene oxidation: thickness-Dependent etching and strong chemical doping, Nano Lett. 8 (2008) 1965–1970.
[29] Q. Liu, J.T. Jin, J.Y. Zhang, $NiCo_2S_4$@graphene as a bifunctional electrocatalyst for oxygen reduction and evolution reactions, ACS Appl. Mater. Interfaces 5 (2013) 5002–5008.
[30] V. Chabot, D.C. Higgins, A. Yu, X. Xiao, Z. Chen, J. Zhang, A review of graphene and graphene oxide sponge: material synthesis and applications to energy and the environment, Energy Environ. Sci. 7 (2014) 1564–1596.
[31] J. Liang, Y. Jiao, M. Jaroniec, S.Z. Qiao, Sulfur and nitrogen dual–doped mesoporous graphene electrocatalyst for oxygen reduction with synergistically enhanced performance, Angew. Chem. Int. Ed. 51 (2012) 11496–11500.
[32] D. Hggins, M.A. Hoque, M.H. Seo, R. Wang, F. Hassan, J.Y. Choi, M. Pritzker, A. Yu, J. Zhang, Z. Chen, Development and simulation of sulfur–doped graphene supported platinum with exemplary stability and activity towards oxygen reduction, Adv. Funct. Mater. 24 (2014) 4325–4336.
[33] L. Lin, M. Li, L.Q. Jiang, Y.F. Li, D.J. Liu, X.Q. He, L.L. Cui, A novel iron (II) polyphthalocyanine catalyst assembled on graphene with significantly enhanced performance for oxygen reduction reaction in alkaline medium, J. Power Sources 268 (2014) 269–278.
[34] R. Li, Z.D. Wei, X.L. Gou, Nitrogen and phosphorus dual-doped graphene/carbon nanosheets as bifunctional electrocatalysts for oxygen reduction and evolution, ACS Catal. 5 (2015) 4133–4142.
[35] G.Q. Zhang, B.Y. Xia, X. Wang, X.W. (David) Lou, Strongly coupled $NiCo_2O_4$–rGO hybrid nanosheets as a methanol–tolerant electrocatalyst for the oxygen reduction reaction, Adv. Mater. 26 (2014) 2408–2412.
[36] M.V. Reddy, G. Prithvi, K.P. Loh, B.V.R. Chowdari, Li storage and impedance spectroscopy studies on Co_3O_4 CoO, and CoN for Li-ion batteries, ACS Appl. Mater. Interfaces 6 (2014) 680–690.
[37] Y. Zhang, B.L. Tao, W. Xing, L. Zhang, Q.Z. Xue, Z.F. Yan, Sandwich–like nitrogen–doped porous carbon/graphene nanoflakes with high–rate capacitive Performance, Nanoscale 8 (2016) 889–7898.
[38] J.K. Kim, Y. Kim, S. Park, H. Ko, Y. Kim, Encapsulation of organic active materials in carbon nanotubes for application to highelectrochemical–performance sodium batteries, Energy Environ. Sci. 25 (2015) 1215–1223.
[39] Y. Matsumoto, E. Sato, Electrocatalytic properties of transition metal oxides for oxygen evolution reaction, Mater. Chem. Phys. 14 (1986) 397–426.
[40] P. Ganesan, M. Prabu, J. Sanetuntikul, S. Shanmugam, Cobalt sulfide nanoparticles grown on nitrogen and sulfur codoped graphene oxide: an efficient electrocatalyst for oxygen reduction and evolution reactions, ACS Catal. 5 (2015) 3625–3637.
[41] S. Ratso, I. Kruusenberg, M. Vikkisk, U. Joost, E. Shulga, I. Kink, T. Kallio, K. Tammeveski, Highly active nitrogen–doped few–layer graphene/carbon nanotube composite electrocatalyst for oxygen reduction reaction in alkaline media, Carbon 73 (2014) 361–370.
[42] M.R. Gao, X. Cao, Q. Gao, S.H. Yu, Nitrogen–doped graphene supported $CoSe_2$ nanobelt composite catalyst for efficient water oxidation, J. ACS Nano 8 (2014) 3970–3978.